Journal of Molecular and Cellular Cardiology 64 (2013) 124–131

Contents lists available at ScienceDirect

Journal of Molecular and Cellular Cardiology

journal homepage: www.elsevier.com/locate/yjmcc

Original article

# SLIT3–ROBO4 activation promotes vascular network formation in human engineered tissue and angiogenesis in vivo

Jonathan D. Paul [a,1], Kareen L.K. Coulombe [b,1], Peter T. Toth [c,d], Yanmin Zhang [d,e], Glenn Marsboom [d], Vytas P. Bindokas [f], David W. Smith [b], Charles E. Murry [b,g,h], Jalees Rehman [d,e,i,*]

[a] Section of Cardiology, Department of Medicine, University of Chicago, Chicago, IL, USA
[b] Department of Pathology, Center for Cardiovascular Biology, Institute for Stem Cell and Regenerative Medicine, University of Washington, Seattle, WA, USA
[c] Research Resources Center, University of Illinois at Chicago, Chicago, IL, USA
[d] Department of Pharmacology, University of Illinois at Chicago, Chicago, IL, USA
[e] Section of Cardiology, Department of Medicine, University of Illinois at Chicago, Chicago, IL, USA
[f] Integrated Microscopy Core Facility, University of Chicago, Chicago, IL, USA
[g] Department of Bioengineering, University of Washington, Seattle, WA, USA
[h] Department of Medicine, Division of Cardiology, University of Washington, Seattle, WA, USA
[i] University of Illinois Cancer Center, University of Illinois at Chicago, Chicago, IL, USA

ARTICLE INFO

*Article history:*
Received 19 March 2013
Received in revised form 27 August 2013
Accepted 6 September 2013

*Keywords:*
Angiogenesis
Revascularization
SLIT–ROBO signaling
Vascular tissue engineering
Mesenchymal stem cells

ABSTRACT

Successful implantation and long-term survival of engineered tissue grafts hinges on adequate vascularization of the implant. Endothelial cells are essential for patterning vascular structures, but they require supportive mural cells such as pericytes/mesenchymal stem cells (MSCs) to generate stable, functional blood vessels. While there is evidence that the angiogenic effect of MSCs is mediated via the secretion of paracrine signals, the identity of these signals is unknown. By utilizing two functionally distinct human MSC clones, we found that so-called "pericytic" MSCs secrete the pro-angiogenic vascular guidance molecule SLIT3, which guides vascular development by directing ROBO4-positive endothelial cells to form networks in engineered tissue. In contrast, "non-pericytic" MSCs exhibit reduced activation of the SLIT3/ROBO4 pathway and do not support vascular networks. Using live cell imaging of organizing 3D vascular networks, we show that siRNA knockdown of SLIT3 in MSCs leads to disorganized clustering of ECs. Knockdown of its receptor ROBO4 in ECs abolishes the generation of functional human blood vessels in an in vivo xenogenic implant. These data suggest that the SLIT3/ROBO4 pathway is required for MSC-guided vascularization in engineered tissues. Heterogeneity of SLIT3 expression may underlie the variable clinical success of MSCs for tissue repair applications.



## 1. Introduction

Cell-based regenerative medicine therapies such as cardiac tissue engineering for ischemic heart disease require adequate vascularization for successful implantation and long-term survival [1,2]. Pericytes are microvascular mural cells which directly interact with endothelial cells to promote endothelial growth and stabilize endothelial networks [3–5]. Importantly, pericytes and mesenchymal stem cells (MSCs) derived from bone marrow or other tissues express a similar array of cell surface markers, thus suggesting that they have significant functional and phenotypic overlap [6–8].

Like pericytes, MSCs can be combined with endothelial cells to enhance the formation of vascular networks [3,9–11]. The currently proposed mechanisms of how MSCs promote angiogenesis are thought to involve the release of angiogenic growth factors [12,13] and stabilization of vascular networks through direct contact. The pericyte function of MSCs remains poorly defined and it is not known whether MSCs release mediators of vascular endothelial cells, similar to those released by pericytes [14]. We sought to explore the contribution of MSCs to EC vascular network formation in vitro and to highly vascularized tissue constructs in vivo, as well as define the role of potential vascular mediators released by MSCs.

*Abbreviations:* DAPT, N-[(3,5-Difluorophenyl)acetyl]-L-alanyl-2-phenyl]glycine-1,1-dimethyletheyl ester; EC, endothelial cell; HAEC, human aortic endothelial cell; HUVEC, human umbilical vein endothelial cell; MSC, mesenchymal stem cell or marrow stromal cell; MSC5, human MSC clonal line HS-5; MSC27a, human MSC clonal line HS-27a; VEGF, vascular endothelial growth factor.

* Corresponding author at: Section of Cardiology, Department of Medicine and Department of Pharmacology, University of Illinois at Chicago, College of Medicine (M/C 868), 835 S. Wolcott Ave. Rm. E403, Chicago, IL 60612, USA. Tel.: +1 312 996 5552; fax: +1 312 996 1225.
*E-mail address:* jalees@uic.edu (J. Rehman).

[1] These two authors contributed equally to the manuscript.

0022-2828 
http://dx.doi.org/10.1016/j.yjmcc.2013.09.005

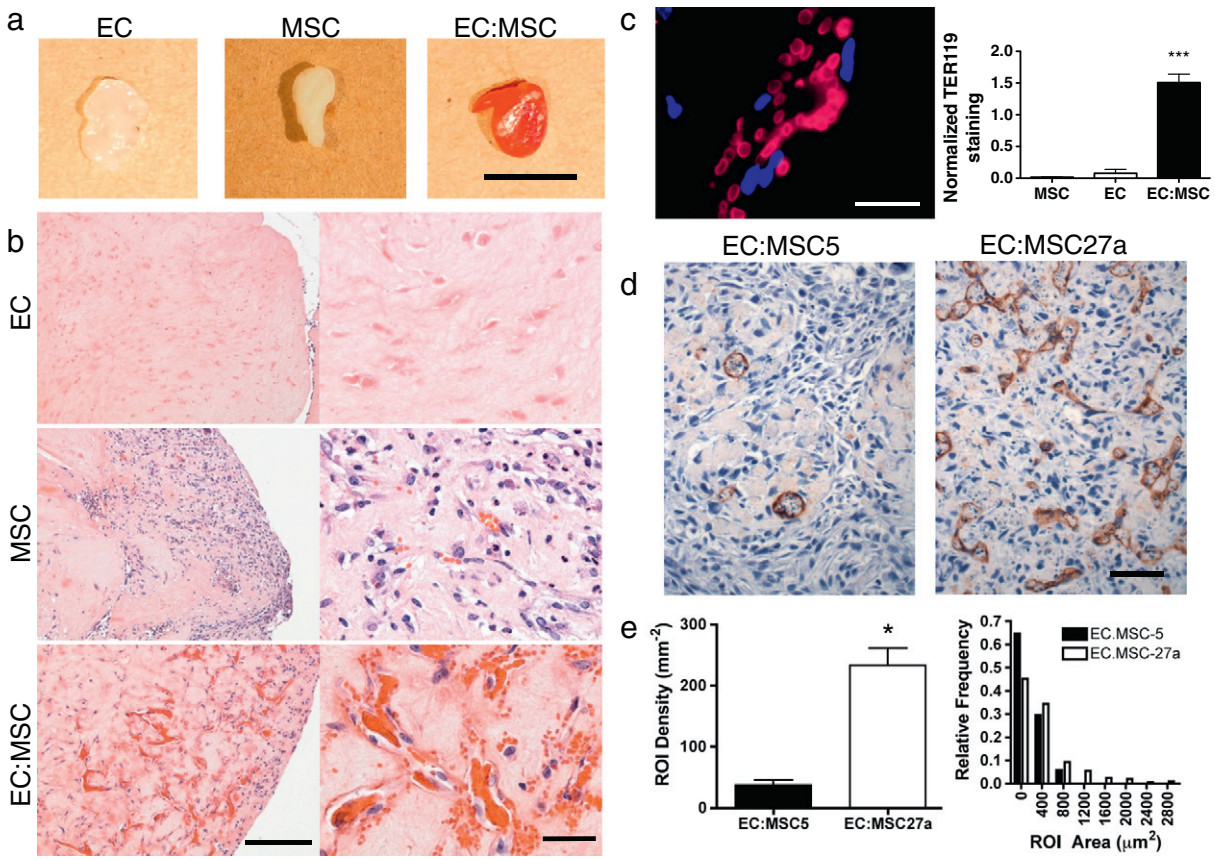


**Fig. 1.** Cross-talk between human endothelial cells (ECs) and human mesenchymal stem cells (MSCs) promotes the formation of vascular networks in engineered tissue and perfused blood vessels in vivo. a, Gross photographs of whole gel explants at 7 days illustrate significant vascularization of gels containing both cell types by the visible red color in EC:MSC explants (right). Scale bar: 5 mm. b, Representative hematoxylin & eosin (H&E) stainings of collagen/fibronectin gel explants after 7 days in vivo show minimal vascularization in implants containing either human ECs (top) or human MSCs (middle). Significant vascularization is observed in implants containing a mixture of the two cell types (bottom) in a 1:1 ratio, where $1 \times 10^6$ total cells were implanted per condition. Scale bar: 200 μm, left; 40 μm, right. c, Red blood cell content in vascularized EC:MSC gel plug, measured by immunostaining against TER-119 (red), is significantly increased in EC:MSC plugs as compared to either cell type alone ($p < 0.001$). Scale bar: 20 μm. Quantification of TER-119 positivity is normalized to the number of DAPI-positive nuclei within each high power field ($n = 18$ (MSC), $n = 4$ (EC), and $n = 16$ (EC:MSC)). d, Immunostaining against CD31 (brown, DAB) in representative scaffold-free engineered tissues after 8 days of in vitro culture containing ECs plus either MSC27a or MSC5 cells shows greatly increased EC networks with MSC27a co-culture. Scale bar: 100 μm. And e, Quantification of in vitro vascularization in engineered tissues by automated detection of regions of interest (ROI) from brown CD31 stain shows increased vascular density (left) and a broader spectrum of structure sizes (right, assessed by individual ROI areas and plotted as a histogram). ROI density is defined as the total number of ROI per area ($mm^2$). ROI area ($\mu m^2$) indicates the area of each ROI outlined (see Supplementary Fig. 1) and is binned and plotted as a relative frequency of the total number of structures (defined as 1.0). The ROI area is a surrogate measure for vessel diameter.

## 2. Materials and methods

### 2.1. Cell culture

Adult human aortic endothelial cells (HAECs, Lonza) and human umbilical vein endothelial cells (HUVECs, Lonza) were maintained in endothelial cell growth medium-2 (EGM-2, Lonza) according to the manufacturer's recommendations and no longer than passage 7. Human bone marrow-derived mesenchymal stem cells (MSCs, Lonza) were maintained in minimal essential medium (α-MEM, Invitrogen) supplemented with 16.5% FBS, 2 mM L-glutamine, and penicillin/streptomycin (final concentration 100 units/ml penicillin and 100 μg/ml streptomycin). MSCs were passaged no more than twice after being thawed before being used in experiments. Human marrow stromal cell clones HS-5 (MSC5) and HS-27a (MSC27a) [15] were cultured in Dulbecco's modified Eagle medium (DMEM, Gibco) with 5% fetal bovine serum (FBS) and 2 mM L-glutamine.

### 2.2. Generation of scaffold-free engineered vascular tissue

Cells were harvested and mixed in a 2:1 ratio (HUVECs:MSCs) without exogenous extracellular matrix proteins to form scaffold-free engineered vascular tissue. Tissue patches were formed in ultra-low attachment six-well plates (Corning) on a rotating orbital shaker at 40 rpm at 37 °C in 50/50 v/v EGM2 and a high-serum medium of KO-DMEM (Gibco) with 20% FBS, 1 mM L-glutamine, 0.1 mM β-mercaptoethanol, and 1% non-essential amino acids as previously described [11,16]. Disk-shaped engineered tissues (circular and about 400 μm thick) formed by hydrodynamic forces and cell adhesion within 2 days and were cultured for up to 8 days with medium changes every other day. Growth factors and small molecule inhibitors were added fresh with media changes and included: recombinant human vascular endothelial growth factor ($VEGF_{165}$, 10 or 100 ng/mL; Millipore) and/or N-[(3,5-Difluorophenyl)acetyl]-L-alanyl-2-phenyl]glycine-1,1-dimethyletheyl ester (DAPT, a gamma-secretase inhibitor, 0.2, 2, or 20 μM; Tocris Bioscience). Dimethyl sulfoxide (DMSO, up to 0.1%) was used as a negative control in experiments requiring DMSO as a solvent for small molecule inhibitors.

### 2.3. Preparation of cellularized three-dimensional gels

For in vitro and in vivo gel experiments, 3D gels were prepared as previously described [17]. Briefly, gel components were placed on ice and combined to the following final concentrations: HEPES, 25 mM;

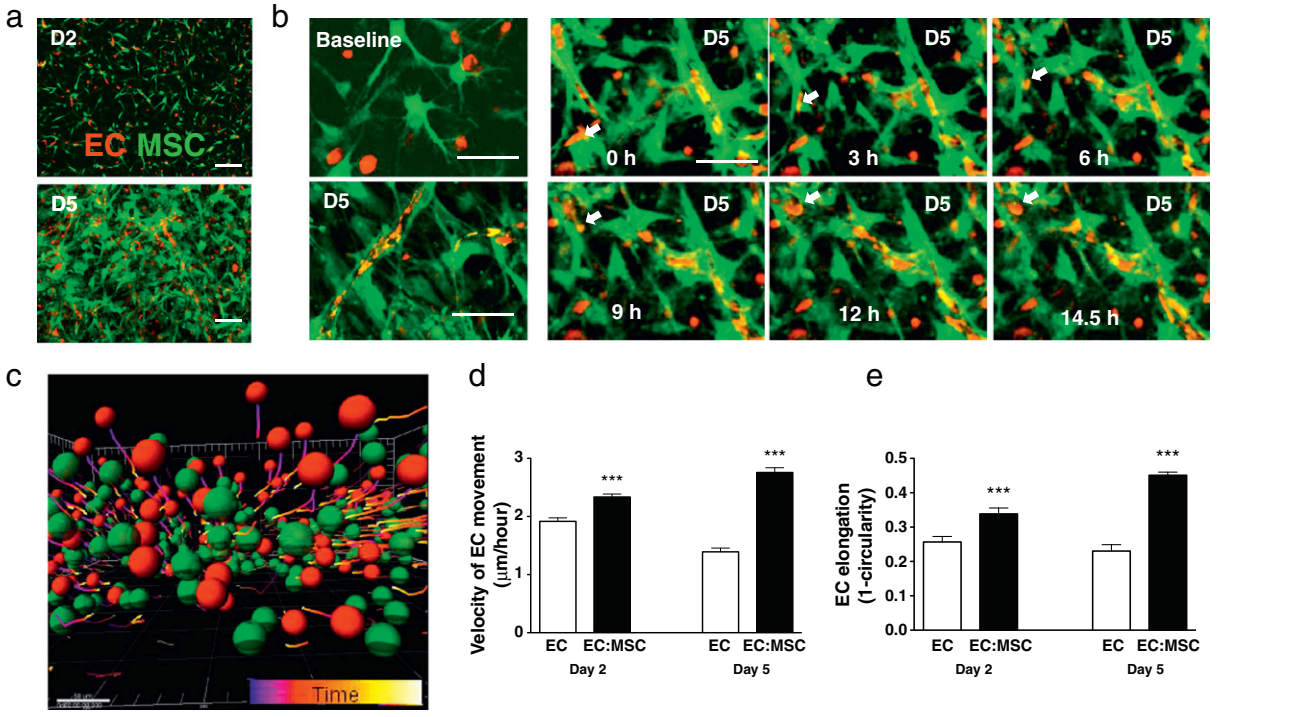


**Fig. 2.** MSCs direct EC movement within primitive vascular networks. a, Live cell imaging of collagen/fibronectin gels containing ECs (red) and MSCs (green) show formation of primitive vascular structures after 5 days (D5) by ECs in close contact with MSCs (a heterogeneous MSC population from Lonza). See Supplementary Video 1 for time-lapse video. Scale bar: 250 μm. b, Time lapse confocal images of an in vitro gel illustrate extensive MSC spreading, MSC cell contact, and EC orientation along MSCs from baseline to day 5 (D5). ECs migrate along MSCs, shown by white arrows which follow an individual EC over time as it migrates along MSCs on day 2 (D2). Scale bar: 100 μm. c, Three-dimensional cell-tracking images taken over a 16 h time period on day 5–6 of EC:MSC in vitro gels. Red and green spheres indicate individual ECs and MSCs, while colored tracks indicate the path of cell movement over time. EC track length and velocity data are derived from these experiments. d, Velocity (μm/h) of EC movement is significantly increased in the presence of MSCs (***$P < 0.001$). And e, ECs assume a more elongated phenotype (where a line is defined as 1.0 and a circle is 0.0) within vascular networks when co-cultured with MSCs at both 2 and 5 days (***$P < 0.001$).

sodium bicarbonate, 1.5 mg/mL; FBS, 10%; human plasma fibronectin (Millipore), 100 μg/mL; rat tail collagen type I (Millipore), 1.5 mg/mL; and EBM-2 supplemented with 10% FBS and 1% penicillin/streptomycin, to bring solution to 0.7 × total volume. Gel pH was adjusted to 7.4 with 1 N NaOH. $1 \times 10^6$ total cells (either alone or at a 1:1 ratio of HAECs and MSCs) were then resuspended in warm EGM-2 medium and mixed with the ice-cold gel solution at a ratio of 2.3:1 (gel:resuspended cells), and immediately plated in glass bottom dishes for analysis by confocal microscopy (final volume 1 ml) or into 24-well dishes (final volume 500 μl) and allowed to polymerize for 15–20 min prior to addition of warm EGM-2 to cover gels for later use in vivo. For in vitro cell tracking experiments, HAECs were labeled with Celltracker™Red CMPTX (Invitrogen) and MSCs labeled with Celltracker™ Green CMFDA (Invitrogen) prior to mixture within gels per manufacturer protocols. All polymerized gels containing cells were placed in an incubator at 37°C overnight prior to conducting in vivo experiments.

### 2.4. Microarray experiments and data analysis

Cellular RNA was harvested from engineered vascular tissue using the RNeasy Mini Kit (Qiagen) with β-mercaptoethanol (1:100) in RLT buffer and on-column DNA digestion, then stored at −80 °C until further use. RNA amplification and labeling was done using the Illumina® TotalPrep™ RNA Amplification Kit (Ambion, Applied Biosystems) according to the manufacturer's instructions. Two biological replicates were run per sample. Samples were human MSC HS-5 (MSC5) and MSC HS-27a (MSC27a) cells (where RNA was harvested from plated cells) and bi-cell patches with HUVECs and either MSC5 or MSC27a cells (with RNA collected after 8 days of culture in engineered tissues). Whole genome expression analysis was performed using the HumanHT-12 V3 BeadChip (Illumina). Expression intensity data was processed with the GenomeStudio Gene Expression Module (Illumina) with background subtraction, and then imported into R/Bioconductor (version 2.15.0 (2012-03-20); R Development Core Team (2012). R: A language and environment for statistical computing. R Foundation for Statistical Computing, Vienna, Austria. ISBN 3-900051-07-0, URL http://www.R-project.org/) for quantile normalization with the quantile.normalize function in the preprocessCore library (Bolstad, B.M. PreprocessCore: A collection of pre-processing functions. R package version 1.18.0), log transformation, and display with the heatmap.2 function of the gplots library (Warnes, G.R. gplots: Various R programming tools for plotting data. R package version 2.10.1. http://CRAN.R-project.org/package=gplots). Fold enrichment was calculated as EC:MSC27a/EC:MSC5 expression levels for bi-cell tissue patches to examine gene expression differences in engineered vascular tissue. Microarray data in both cultured cells and in engineered tissues was validated by qPCR for the genes SLIT3 and ROBO4. Microarray data are MIAME compliant, and can be accessed in NCBI's Gene Expression Omnibus [18] with GEO Series accession number GSE48302 (http://www.ncbi.nlm.nih.gov/geo/query/acc.cgi?acc=GSE48302).

### 2.5. RNA isolation and gene expression profiling

RNA was isolated from monolayer cells or 3-dimensional gels using a Purelink™ RNA Mini Kit (Invitrogen). Dispersion of 3-dimensional gels was accomplished by vortexing in lysis buffer until the gel was completely dissolved. cDNA was synthesized using the High Capacity cDNA Reverse Transcription Kit (Applied Biosystem). RNA was isolated from engineered tissues using the RNeasy Mini Kit (Qiagen) with β-mercaptoethanol (1:100) in RLT buffer and on-column DNA digestion.

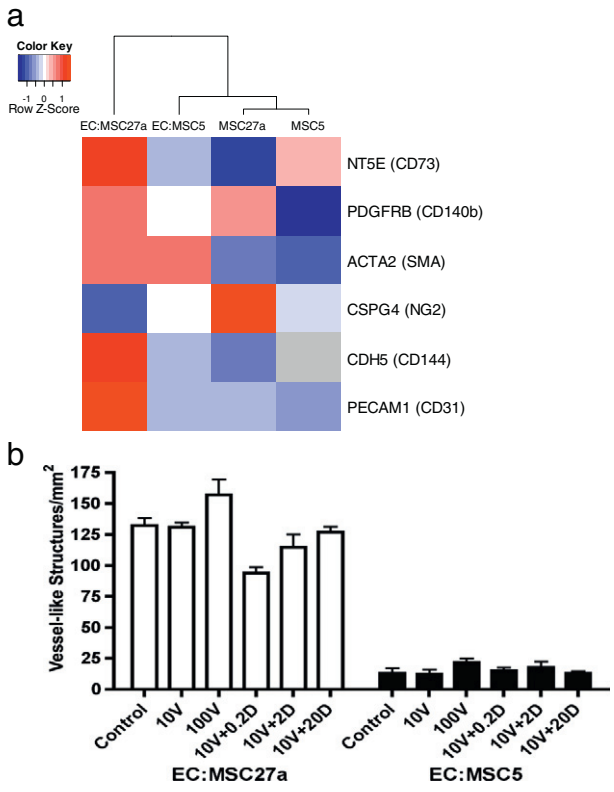


**Fig. 3.** MSC27a cells exhibit a pericytic phenotype, and manipulation of known angiogenic pathways does not significantly affect vascular formation in engineered tissue constructs. a, Array expression data heatmap of pericyte and EC markers in two distinct MSC clones (MSC5 and MSC27a) and in corresponding engineered tissues also containing ECs (labeled with "gene name (protein)") shows a general trend towards increased expression in EC:MSC27a tissues. Scale indicates highly expressed (red) or minimally expressed (blue) genes based on a row-level z-score calculated as $(x-x_{mean})/StDev$ (where values are expressed as $\log_2$). Gray color indicates expression was not detected. Note that CD144 and CD31 were highly expressed in EC:MSC27a patches compared to EC:MSC5 patches, likely due to improved EC survival in the former engineered tissues. And b, Manipulation of known angiogenic pathways VEGF and NOTCH in engineered tissues with VEGF-$A_{165}$ at 10 or 100 ng/ml (10 V or 100 V), or with 10 ng/ml VEGF-$A_{165}$ and DAPT at 0.2, 2, or 20 μM (10 V + 0.2D, 2D, or 20D, respectively) showed no changes in vessel structure development after 8 days in culture (n = 3 per group, P = not significant by ANOVA).

cDNA was generated using random primers (Promega) and Superscript III Reverse Transcriptase (Invitrogen). Real-time qRT-PCR analysis was performed using a 7900HT Fast Real-Time PCR System (Applied Biosystems) using either SYBR®-Green or TaqMan® based detection systems (Applied Biosystems). Data were normalized to B2M or HPRT1 expression (endogenous control) and fold changes in gene expression were determined by the $2^{-\Delta\Delta CT}$ method. PCR primer sequences are available upon request.

### 2.6. Confocal microscopy/time lapse videos

3D gels were imaged with a Zeiss 510META confocal laser scanning microscope (Carl Zeiss Microimaging, Thornwood, NY, USA) equipped with an environmental chamber to maintain humidity, temperature (37 °C) and $CO_2$ (5%). CellTracker Green was excited at 488 nm and CellTracker Red was excited at 561 nm. Excitation and acquisition at both wavelengths were carried out simultaneously to minimize motion artifact. To be able to image cells in the entire thickness of the gel, a long working distance 10×/0.30 NA Plan-Neofluar objective was selected (Zeiss Microimaging). To prevent photobleaching, low laser power, high scan speed and only 2 scans for averaging were used. Other imaging parameters were adjusted to optimize the trade-off between imaging time and spatial resolution. When recording time-lapse videos for network development, z-stacks were generated every 32 min (1024 × 1024 × 80 sample size, 0.879 × 0.879 × 5.8 $\mu m^3$ voxel size). The resolution was increased when stacks were recorded for co-localization analyses (1024 × 1024 × 60 sample size, 0.879 × 0.879 × 3.53 $\mu m^3$ voxel size or 2000 × 2000 × 55 sample size, 0.45 × 0.45 × 2.81 $\mu m^3$ voxel size). High-resolution images from gels were acquired with a 40×/1.1NA water immersion objective (0.112 × 0.112 $\mu m^2$ pixel size) (Zeiss Microimaging). Imaris 3D/4D image processing and analysis software (Bitplane Inc., South Windsor, CT) was used for automated tracking of endothelial cells and for 3D co-localization analysis. EC/MSC co-localization was determined with thresholded Mander's coefficients.

### 2.7. Cell transplantation

All animal experiments were approved by the Institutional Animal Care and Use Committee (IACUC) of the University of Chicago. Gels containing 1 × $10^6$ total cells were subcutaneously implanted bilaterally into the ventral surface of adult female NOD SCID mice after overnight incubation. To accomplish this, mice were anesthetized with isoflurane and the implantation site cleaned and shaved. A small subcutaneous pocket was made for each gel, and the wound closed using skin staples. After 7 days, animals were sacrificed, and the gel implants were harvested.

### 2.8. Statistical analysis

Data was analyzed by using a Student's unpaired *t* test or one-way analysis of variance (ANOVA). P values <0.05 were considered statistically significant.

See Online Data Supplement–Methods for details on cell surface marker analysis, siRNA transfection, proliferation assays, and immunohistochemistry.

## 3. Results

We began by studying angiogenesis in an in vivo model where human cells were implanted subcutaneously in a collagen/fibronectin gel. Delivery of either endothelial cells or bone marrow MSCs alone resulted in minimal vascular network formation, whereas combining human MSCs and human ECs resulted in profound vascularization (Fig. 1a,b). The functionality of blood vessels was assessed by measuring the red blood cell content in the explanted tissues. Tissues containing both ECs and MSCs showed more than a 15-fold enhancement of red blood cell content (Fig. 1c). Thus, MSC–EC co-culture robustly supports vascularization in this in vivo angiogenesis model.

In order to study vascular development and EC–MSC interactions, we used in vitro engineered tissue patches formed without exogenous scaffold materials so that they maintain a high cellular density [11]. While the in vivo implants were performed with commercially available MSCs (Lon–MSCs, Lonza), for these in vitro studies we exploited two human bone marrow-derived MSC clones (HS-27a, designated here as "MSC27a" and HS-5, designated here as "MSC5"). These clones have been previously characterized as having distinct functional effects: MSC5 cells have a fibroblastic growth pattern and support proliferation of hematopoietic progenitors in co-culture, whereas MSC27a cells grow in an epithelioid pattern and do not support hematopoietic expansion.[19,20] In engineered tissue patches with ECs and MSCs, only the MSC27a line was able to support the formation of dense EC networks with a broader range of vessel structure sizes (Fig. 1d,e and Supplementary Fig. 1). Engineered tissue patches with ECs and MSC5 cells had a low density of vessel structures with a more narrow size range. This finding not only points to the pericytic nature of MSC27a

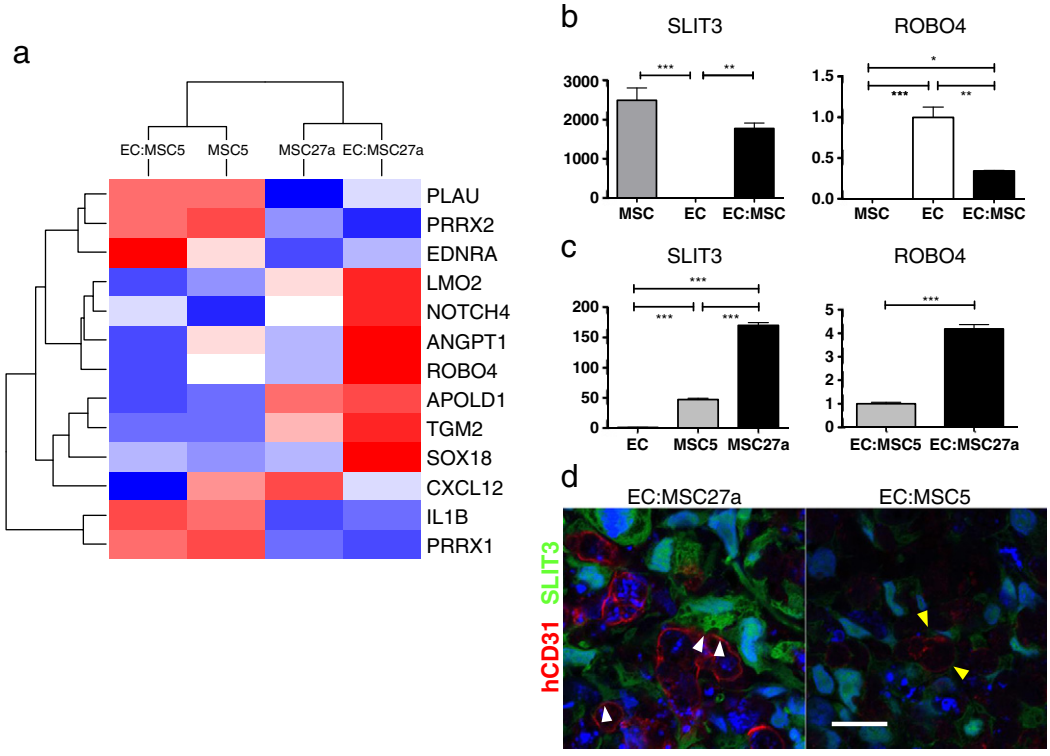


**Fig. 4.** Whole genome microarray revealed seven genes strongly upregulated during MSC-mediated vascular development in engineered tissue and led to identification of SLIT3/ROBO4 as a leading candidate pathway. a, Microarray gene expression profiling of cultured MSC clones (MSC5 and MSC27a) and in vitro scaffold-free engineered tissues EC:MSC5 and EC:MSC27a was used to identify 13 genes changing >8-fold in EC:MSC27a versus EC:MSC5 engineered tissues and associated with gene ontology terms "blood vessel morphogenesis", "blood vessel development", and "vasculature development" (P-values < 0.003 and annotation cluster enrichment score of 2.5) by DAVID functional annotation clustering analysis. Scale is as in Fig. 3a and demonstrates that 7 genes are strongly upregulated in the vascular EC:MSC27a engineered tissues (red color), including ANGPT1, NOTCH4, and ROBO4. b, SLIT3 and ROBO4 mRNA expression by qPCR after 48 h in vitro culture of MSCs, ECs, or 1:1 combination of the two cell types demonstrates MSC-specific expression of SLIT3 and EC-specific expression of ROBO4 (n = 3 per group; ***P < 0.001, **P < 0.01, and *P < 0.05). c, SLIT3 mRNA expression by qPCR is significantly higher in MSC27a cells compared to MSC5 cells (n = 3 per group; ***P < 0.001). Further, ROBO4 mRNA expression is more than four-fold higher in EC:MSC27a as compared to EC:MSC5 engineered tissues (n = 3 per group, ***P < 0.001). d, Engineered vascular tissue in vitro shows ample SLIT3 (green) in EC:MSC27a tissues (left) and reduced SLIT3 in EC:MSC5 tissues (right; confocal images taken with same laser settings). SLIT3-positive MSC27a cells extend processes (white arrowheads) toward human CD31-positive ECs (red) in a pericyte-like manner. No overlap between SLIT3 and hCD31 signals suggests that only MSC27a cells produce SLIT3. The surviving endothelial cells in EC:MSC5 tissues may be supported by MSCs expressing low levels of SLIT3 with projections towards the ECs (yellow arrowheads). Scale bar: 20 μm.

cells, but also highlights that distinct human MSCs have a varying propensity to promote vascular network formation.

We next followed EC:MSC vascular network formation over 5 days in 3D collagen/fibronectin gels to track the behavior of individual cells using time-lapse confocal microscopy (Fig. 2a). After 2 days, Lon–MSCs (green) and ECs (red) remained widely distributed within the gel, and by day 5, ECs oriented along tracks created by MSCs. Live cell imaging revealed significant movement of ECs along these scaffold-like tracks (Fig. 2b, Supplementary Video 1). The velocity of EC movement over time was quantified, and the presence of MSCs significantly enhanced the speed of EC movement at both 2 and 5 days (Fig. 2c,d). The morphology of ECs also changed in the presence of MSCs, with ECs becoming significantly more elongated and less circular by day 5 in the presence of MSCs (Fig. 2e).

Interestingly, examination of clonal MSC lines showed that MSC27a cells express relatively higher levels of most classic pericyte markers such as NG2 and PDGFRB, when compared to the MSC5 cells (Fig. 3a, Supplementary Table 1). When the MSC lines were combined with ECs in engineered tissue patches, this difference was even further enhanced with marked upregulation of the pericyte marker CD73 in EC:MSC27a tissue patches. On the other hand, MSC5 cells not only expressed lower levels of most pericyte markers, but they did not augment the expression of these genes upon combination with ECs. Together, these data suggest that ECs influence the maturation of MSC27a cells into vascular pericytes, but ECs and MSC5 cells exhibit less synergy. The heterogeneous Lon–MSCs expressed surface markers that are typically found on both MSCs and pericytes (Supplementary Fig. 2a), confirming the presence of at least some pericyte-like cells in this mixed population.

To better understand what controls vessel formation in engineered tissue, we assessed vascular structure formation after addition of known angiogenic factors. Addition of VEGF and inhibition of NOTCH signaling with a small molecule γ-secretase inhibitor (DAPT) did not have any significant impact on the formation of vascular structures in engineered tissue containing either MSC5 or MSC27a cells (Fig. 3b). These data suggested that, although VEGF and DAPT can promote angiogenesis in vitro and in vivo [21], neither VEGF nor inhibition of NOTCH signaling were sufficient to explain the different abilities of MSCs to promote vascular network formation in engineered tissue.

Whole genome microarray analysis of MSC clones and EC:MSC engineered tissue patches was performed to assess differences in MSC clones and changes in gene expression profiles upon co-culture with ECs. To better understand the pathways involved in the angiogenic contribution of MSC27a compared to MSC5 cells, microarray analysis identified 423 genes with >8-fold change in expression (Supplementary Fig. 2b). Of these, 13 genes were found to be enriched in the gene ontologies "angiogenesis", "blood vessel morphogenesis", "blood vessel development", and "vasculature development" by DAVID analysis. The hierarchical clustering of the microarray heatmap (Fig. 4a) by similarity of gene expression profiles revealed several key findings. First, in EC:MSC27a tissues, there was significant upregulation of classic "pro-angiogenic" genes, such as NOTCH4 and angiopoietin 1 (ANGPT1). Also clustered in this group and showing the same expression profile was ROBO4, the endothelial-specific receptor for SLIT soluble ligands.

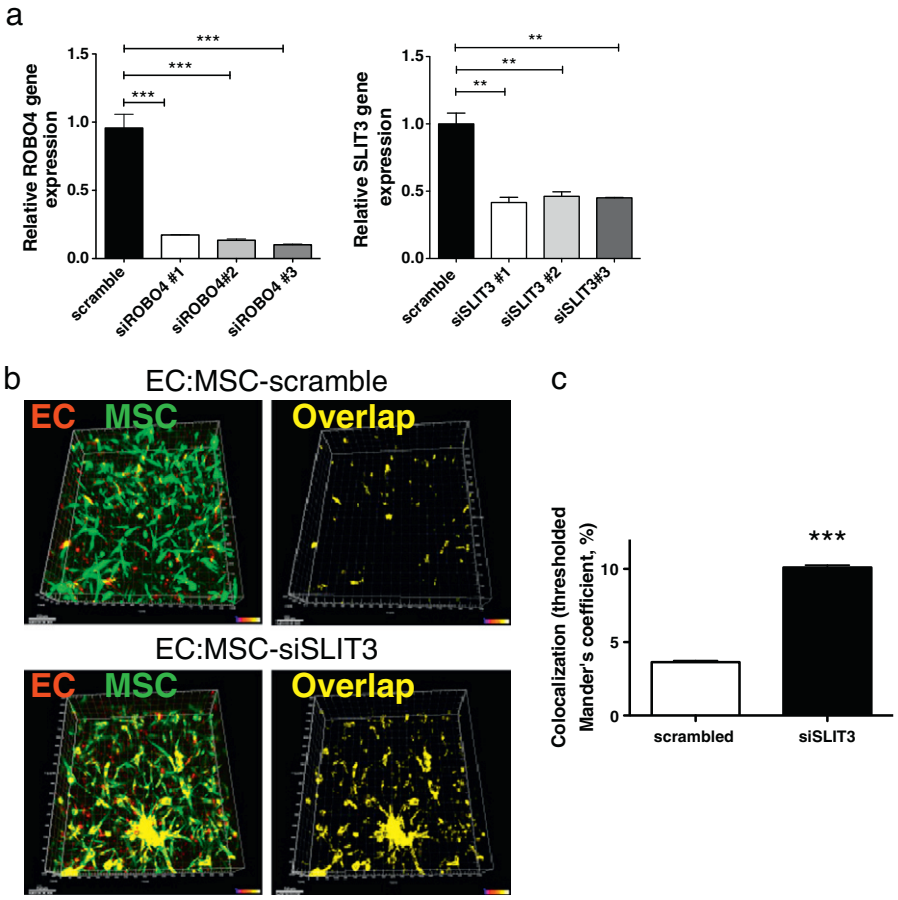


**Fig. 5.** SLIT3/ROBO4 signaling is required for efficient vascular network formation in vitro. a, Gene expression levels of SLIT3 (left) and ROBO4 (right) in MSCs and ECs, respectively, each transfected with 3 different siRNAs against the target gene show significant knockdown by qPCR. b, ECs (red) were co-cultured in three-dimensional in vitro gels with MSCs (green) after siRNA infection of MSCs with a control siRNA (scramble, top) or siRNA against SLIT3 (siSLIT3, bottom). SLIT3 knockdown caused cell aggregation, identified as large overlapping cell clusters comprised of both cell types (yellow, right), suggesting that SLIT3 acts as a repellant signal or mobility signal for ECs during vessel formation. And c, Quantification of this effect, expressed as co-localization, shows a significant increase in co-localized cells in the EC:MSC-siSLIT3 group compared to scramble control (***$P < 0.001$).

Furthermore, a similar expression profile was found, albeit at lower expression levels, for vascular endothelial growth factor A (VEGFA) and SLIT3, a ligand for ROBO receptors which has also been shown to promote angiogenesis during organ development [22] (Supplementary Table 2).

The recently identified role of the SLIT/ROBO pathway in promoting angiogenesis during organ development led us to investigate whether SLIT3–ROBO4 signaling may be an important determinant of vascular network formation in EC–MSC gels and engineered tissues. In gel assays containing ECs-only, MSCs-only, or co-cultured ECs and MSCs (in a 1:1 ratio), SLIT3 mRNA was nearly exclusively expressed in MSCs whereas ROBO4 expression was EC-specific (Fig. 4b). SLIT3 and ROBO4 expression were reduced by about half with co-culture, likely reflecting the dilution of total mRNA by the mRNA from the other cell type. Increased expression of SLIT3 in MSC27a as compared to MSC5 cells was confirmed by qPCR (Fig. 4c), and in engineered tissue patches, SLIT3 expression was confirmed at the protein level (Fig. 4d), where EC:MSC27a patches contained intense SLIT3 staining that did not colocalize with ECs (stained by human CD31). In contrast, EC:MSC5 patches exhibited minimal staining for SLIT3. The receptor for SLIT3, ROBO4, was expressed to a higher degree in EC:MSC27a patches as compared to EC:MSC5 patches (Fig. 4c), possibly due to reduced survival of ECs in the EC:MSC5 patches. Potential changes in cell numbers during co-culture were a limitation of this analysis, however the striking differences in SLIT3 protein levels between MSC5 and MSC27a patches warranted further investigation. Furthermore, the SLIT3-positive MSC27a cells appeared to extend processes toward the human CD31-positive ECs in a pericyte-like manner (white arrowheads, Fig. 4d), possibly indicative of a role in maintaining EC structure and function. Expression of SLIT2, another well-studied SLIT ligand, was not markedly different between any of the in vivo cell constructs (Supplementary Fig. 3). Based on these data, we hypothesized that the SLIT3/ROBO4 signaling pathway is active between ECs and MSCs in co-cultured tissues and controls vascular assembly.

To determine the necessity of SLIT3/ROBO4 signaling in MSC-guided vessel formation, siRNA knockdown of SLIT3 or ROBO4 was performed. Sufficient suppression was achieved for SLIT3 (60% reduction) and ROBO4 (80% reduction; Fig. 5a) and MSC proliferation was not impacted by siRNA knockdown of SLIT3 (Supplementary Fig. 4). Instead, suppression of SLIT3 in MSCs resulted in significant aggregation or clustering of MSCs and ECs in in vitro gel assays at 2 days as measured by 3D colocalization analysis (Fig. 5b,c). The observed cell clustering suggests that SLIT3 released by MSCs may act as a repellent in this context, similar to its role in neural interactions. This repellent function may provide an important counterbalance to the attractant factors such as VEGF, thus enabling ECs to migrate in the three-dimensional gel and to form vascular networks. The functional importance of SLIT3/ROBO4 was also evaluated in vivo. Following siRNA knockdown of either SLIT3 in MSCs or ROBO4 in ECs, subcutaneous implantation of co-cultured cells in collagen/fibronectin gels showed a profound suppression of functional vascularization (Fig. 6). These data demonstrate that SLIT3 and ROBO4 are required for vessel formation in EC:MSC tissues in vitro and in vivo.

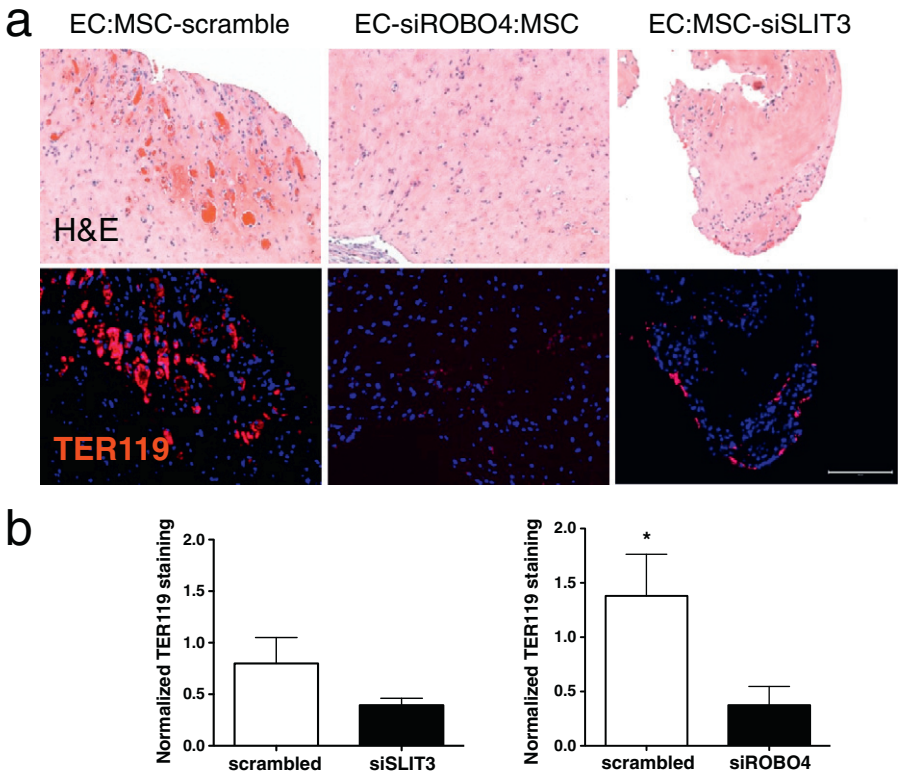


**Fig. 6.** Inhibition of SLIT3/ROBO4 signaling in vivo leads to significantly decreased functional blood vessel formation. a, Perfused vasculature as identified in H&E stained sections (top) and by TER119 staining of red blood cells (bottom) in control EC:MSC explants (left) is reduced with siRNA knockdown of ROBO4 in ECs (EC-siROBO4:MSC, middle) or with siRNA knockdown of SLIT3 in MSCs (EC:MSC-siSLIT3, right). Scale bar: 200 μm. And b, Quantification of TER119-positive area (normalized to number of nuclei) shows reduced vasculature formation for SLIT3 and ROBO4 knockdown (*$P < 0.05$).

## 4. Discussion

Our findings establish a novel role for the SLIT3/ROBO4 pathway in engineered vascular tissue and in an in vivo angiogenesis assay where EC–MSC interactions are required. While this pathway has been well described in neurovascular guidance [22–26], recent studies also implicate the SLIT/ROBO pathway in organogenesis, vascular homeostasis, and tumor angiogenesis [26–29]. It is clear that specific ligand-receptor pairs have unique outcomes in different contexts and signal through different mechanisms [30–33]. For example, SLIT2 released from tumor cells acts as an attractant of ECs for tumor angiogenesis that is ROBO1-dependent [29]. However, when SLIT2 is bound to ROBO4 in normal vascular homeostasis, this is a stabilizing signal for the vasculature to inhibit VEGF-induced EC migration, tube formation, and permeability in vitro and prevent pathologic angiogenesis in the eye [26]. In contrast, when SLIT3 binds ROBO4, EC motility is stimulated in vitro and angiogenesis is enhanced in vivo [22]. Further, the SLIT3 knockout mouse displays severe developmental angiogenic defects in the diaphragm [22,28]. Our results corroborate that SLIT3/ROBO4 modulates angiogenesis via enhanced EC motility (Fig. 2d), and further suggest that SLIT3/ROBO4 acts to prevent EC aggregation (Fig. 5b,c) and promote branched patterning. Most importantly, our results extend the previously established roles of SLIT/ROBO signaling in tumor angiogenesis or during organ development by demonstrating that this pathway may be an important target in vascular tissue engineering using ECs and MSCs.

The release of SLIT3 from MSCs that successfully support angiogenesis (i.e. MSC27a cells) also suggests that this pathway may be indicative of the pericyte-like phenotype of certain MSCs. Importantly, we observed that MSC clones have distinct SLIT3 expression profiles and vasculogenic potential. MSC27a cells, in addition to producing large amounts of SLIT3, also express high levels of the pericyte marker NG2 (Fig. 3a). Interestingly, when MSC27a cells are combined with ECs, both the mature MSC marker CD73 and the vascular smooth muscle cell marker α-smooth muscle actin (SMA) are upregulated (Fig. 3a), suggesting the presence of a more mature vascular stroma. This synergism between ECs and MSC27a was not seen with ECs and MSC5 cells. Further, organization of vascular structures in our engineered tissue constructs, while greatly influenced by the specific MSC clone, was not further affected by manipulation of either VEGF or NOTCH, both recognized to be critical angiogenic factors (Fig. 3b).

While there is significant interest in using autologous MSCs for vascular tissue regeneration therapies, variation among patients and properties of a heterogeneous MSC population need to be considered. Functional testing of MSCs may be necessary to assess SLIT3 expression levels and the ability of the MSCs to generate functional vessels in engineered tissue prior to use of these cells for vascular therapies. Unlike the immortalized clonal MSC lines such as MSC5 or MSC27a, primary MSCs obtained from a patient likely represent a heterogeneous mixture of MSCs, much like the commercially available Lon–MSCs that were used in this study. The inhibition of vascular network formation by suppression of SLIT3 in primary MSCs (Fig. 6) demonstrates that SLIT3/ROBO4 activation is not only important in MSC clones but also in heterogeneous primary MSCs derived from human subjects or patients. Such heterogeneous MSC cultures may contain varying fractions of "pericyte-like" MSCs which support vascular network formation. The heterogeneous Lon–MSCs exhibited a pericyte phenotype and were able to promote SLIT3/ROBO4 dependent vascular network formation in vitro and in vivo, but this may not necessarily apply to all heterogeneous MSC populations obtained from patients. Clinical studies may need to identify whether genetic traits or cardiovascular disease in an individual can impact the phenotype of MSCs. If MSCs are identified that are deficient in SLIT3 or do not have a pericyte-like phenotype,

these deficiencies may need to be addressed prior to using the cells for tissue engineering and regenerative therapies.

## 5. Conclusions

In conclusion, we demonstrate that a pericyte-like function of MSCs supports the formation of vessel-like structures in vitro and vasculature in vivo. We show that SLIT3/ROBO4 signaling is required for formation of EC networks in EC–MSC tissue in vitro and perfused vessels in vivo in a gel plug angiogenesis assay. Finally, distinct MSC clones show a baseline variability in expression of SLIT3, suggesting that MSC phenotype is an important consideration when assessing cells for regenerative vascular therapies.

## Funding Sources

This work was supported in part by NIH-R01-GM094220 (JR), NIH-K08-HL080082 (JR), NIH-R01-HL084642 (CEM), NIH-P01-HL094374 (CEM), NIH-P01-GM81619 (CEM), NIH-U01-HL100405 (CEM), NIH-T32-HL007381 (JDP), NIH-T32-HL007312 (KLK), and the Heart Research Foundation (JR).

## Disclosures

BEAT Biotherapeutics Corporation (CEM).

Supplementary data to this article can be found online at http://dx.doi.org/10.1016/j.yjmcc.2013.09.005.

## Acknowledgments

We gratefully acknowledge Ron Seifert and Peter Bache-Wiig for the expert histology and imaging assistance, and David Feldman for the image analysis assistance.

## References

[1] Stevens KR, Kreutziger KL, Dupras SK, Korte FS, Regnier M, Muskheli V, et al. Physiological function and transplantation of scaffold-free and vascularized human cardiac muscle tissue. Proc Natl Acad Sci U S A 2009;106:16568–73.
[2] Levenberg S, Rouwkema J, Macdonald M, Garfein ES, Kohane DS, Darland DC, et al. Engineering vascularized skeletal muscle tissue. Nat Biotechnol 2005;23:879–84.
[3] Dar A, Domev H, Ben-Yosef O, Tzukerman M, Zeevi-Levin N, Novak A, et al. Multipotent vasculogenic pericytes from human pluripotent stem cells promote recovery of murine ischemic limb. Circulation 2012;125:87–99.
[4] Gaengel K, Genove G, Armulik A, Betsholtz C. Endothelial-mural cell signaling in vascular development and angiogenesis. Arterioscler Thromb Vasc Biol 2009;29:630–8.
[5] Simonavicius N, Ashenden M, van Weverwijk A, Lax S, Huso DL, Buckley CD, et al. Pericytes promote selective vessel regression to regulate vascular patterning. Blood 2012;120(7):1516–27.
[6] Crisan M, Yap S, Casteilla L, Chen CW, Corselli M, Park TS, et al. A perivascular origin for mesenchymal stem cells in multiple human organs. Cell Stem Cell 2008;3:301–13.
[7] da Silva Meirelles L, Caplan AI, Nardi NB. In search of the in vivo identity of mesenchymal stem cells. Stem Cells 2008;26:2287–99.
[8] Paquet-Fifield S, Schluter H, Li A, Aitken T, Gangatirkar P, Blashki D, et al. A role for pericytes as microenvironmental regulators of human skin tissue regeneration. J Clin Invest 2009;119:2795–806.
[9] Boyd NL, Nunes SS, Jokinen JD, Krishnan L, Chen Y, Smith KH, et al. Microvascular mural cell functionality of human embryonic stem cell-derived mesenchymal cells. Tissue Eng Part A 2011;17:1537–48.
[10] Butler MJ, Sefton MV. Cotransplantation of adipose-derived mesenchymal stromal cells and endothelial cells in a modular construct drives vascularization in SCID/bg mice. Tissue Eng Part A 2012;18:1628–41.
[11] Kreutziger KL, Muskheli V, Johnson P, Braun K, Wight TN, Murry CE. Developing vasculature and stroma in engineered human myocardium. Tissue Eng Part A 2011;17:1219–28.
[12] Gnecchi M, He H, Liang OD, Melo LG, Morello F, Mu H, et al. Paracrine action accounts for marked protection of ischemic heart by Akt-modified mesenchymal stem cells. Nat Med 2005;11:367–8.
[13] Rehman J, Traktuev D, Li J, Merfeld-Clauss S, Temm-Grove CJ, Bovenkerk JE, et al. Secretion of angiogenic and antiapoptotic factors by human adipose stromal cells. Circulation 2004;109:1292–8.
[14] Daneman R, Zhou L, Kebede AA, Barres BA. Pericytes are required for blood–brain barrier integrity during embryogenesis. Nature 2010;468(7323):562–6.
[15] Roecklein BA, Torok-Storb B. Functionally distinct human marrow stromal cell lines immortalized by transduction with the human papilloma virus E6/E7 genes. Blood 1995;85:997–1005.
[16] Stevens KR, Pabon L, Muskheli V, Murry CE. Scaffold-free human cardiac tissue patch created from embryonic stem cells. Tissue Eng Part A 2009;15:1211–22.
[17] Mead LE, Prater D, Yoder MC, Ingram DA. Isolation and Characterization of Endothelial Progenitor Cells from Human Blood. Current Protocols in Stem Cell Biology 2008;6:2C.1.1–2C.1.27.
[18] Edgar R, Domrachev M, Lash AE. Gene Expression Omnibus: NCBI gene expression and hybridization array data repository. Nucleic Acids Res 2002;30:207–10.
[19] Graf L, Iwata M, Torok-Storb B. Gene expression profiling of the functionally distinct human bone marrow stromal cell lines HS-5 and HS-27a. Blood 2002;100:1509–11.
[20] Iwata M, Awaya N, Graf L, Kahl C, Torok-Storb B. Human marrow stromal cells activate monocytes to secrete osteopontin, which down-regulates Notch1 gene expression in CD34+ cells. Blood 2004;103(12):4496–502.
[21] Wozniak LJ, Hussain SA, Goldman H, Hand IL. The cardiothoracic ratio in AGA and SGA very low birth weight newborn infants. J Perinatol 2006;26:769–71.
[22] Zhang B, Dietrich UM, Geng JG, Bicknell R, Esko JD, Wang L. Repulsive axon guidance molecule Slit3 is a novel angiogenic factor. Blood 2009;114:4300–9.
[23] Adams RH, Eichmann A. Axon guidance molecules in vascular patterning. Cold Spring Harb Perspect Biol 2010;2:a001875.
[24] Dickson BJ. Molecular mechanisms of axon guidance. Science 2002;298:1959–64.
[25] Jaworski A, Tessier-Lavigne M. Autocrine/juxtaparacrine regulation of axon fasciculation by Slit–Robo signaling. Nat Neurosci 2012;15:367–9.
[26] Jones CA, London NR, Chen H, Park KW, Sauvaget D, Stockton RA, et al. Robo4 stabilizes the vascular network by inhibiting pathologic angiogenesis and endothelial hyperpermeability. Nat Med 2008;14:448–53.
[27] Park KW, Morrison CM, Sorensen LK, Jones CA, Rao Y, Chien CB, et al. Robo4 is a vascular-specific receptor that inhibits endothelial migration. Dev Biol 2003;261:251–67.
[28] Liu J, Zhang L, Wang D, Shen H, Jiang M, Mei P, et al. Congenital diaphragmatic hernia, kidney agenesis and cardiac defects associated with Slit3-deficiency in mice. Mech Dev 2003;120:1059–70.
[29] Wang B, Xiao Y, Ding BB, Zhang N, Yuan X, Gui L, et al. Induction of tumor angiogenesis by Slit–Robo signaling and inhibition of cancer growth by blocking Robo activity. Cancer Cell 2003;4:19–29.
[30] Sheldon H, Andre M, Legg JA, Heal P, Herbert JM, Sainson R, et al. Active involvement of Robo1 and Robo4 in filopodia formation and endothelial cell motility mediated via WASP and other actin nucleation-promoting factors. FASEB J 2009;23:513–22.
[31] Jones CA, Nishiya N, London NR, Zhu W, Sorensen LK, Chan AC, et al. Slit2–Robo4 signalling promotes vascular stability by blocking Arf6 activity. Nat Cell Biol 2009;11:1325–31.
[32] Marlow R, Binnewies M, Sorensen LK, Monica SD, Strickland P, Forsberg EC, et al. Vascular Robo4 restricts proangiogenic VEGF signaling in breast. Proc Natl Acad Sci U S A 2010;107:10520–5.
[33] Hussain SA, Piper M, Fukuhara N, Strochlic L, Cho G, Howitt JA, et al. A molecular mechanism for the heparan sulfate dependence of slit–robo signaling. J Biol Chem 2006;281:39693–8.